Characterization of the pressure loss coefficient using a building block approach with application to by-pass pigs

Hendrix, Maurice; Liang, X; Breugem, Wim-Paul; Henkes, Ruud

DOI
10.1016/j.petrol.2016.11.009

Publication date
2017

Document Version
Final published version

Published in
Journal of Petroleum Science and Engineering

Journal of Petroleum Science and Engineering 150 (2017) 13–21

Contents lists available at ScienceDirect

Journal of Petroleum Science and Engineering

journal homepage: www.elsevier.com/locate/petrol

Characterization of the pressure loss coefficient using a building block approach with application to by-pass pigs

M.H.W. Hendrix[a,*], X. Liang[a], W.-P. Breugem[a], R.A.W.M. Henkes[a,b]

[a] Laboratory for Aero and Hydrodynamics, Delft University of Technology, Leeghwaterstraat 21, Delft, 2628 CA, The Netherlands
[b] Shell Technology Centre Amsterdam, Amsterdam, The Netherlands

ARTICLE INFO

Keywords:
Pressure loss coefficient
By-pass pig
CFD

ABSTRACT

A building block strategy for modelling the pressure loss coefficient of flow through a complex geometry is presented. The approach relies on decomposing a complex flow geometry into geometrical building blocks of which the pressure loss coefficients are characterized individually. The different contributions are subsequently combined to describe the pressure loss of the geometry as a whole. This approach is applied and tested to an industrially relevant application: a by-pass pig (Pipeline Inspection Gauge). This is a cylindrical device that travels inside a pipeline and is commonly used in the oil and gas industry for pipeline maintenance. An important factor in determining the ultimate velocity of the device is the pressure drop over the by-pass pig, which is characterized by a pressure loss coefficient due to the by-passing fluids. In this study the pressure loss coefficient of three frequently used by-pass pig geometries in a single phase pipeline is investigated with Computational Fluid Dynamics (CFD). The CFD results are used to validate the simple building block approach for systematic modelling of the pressure loss through the by-pass pigs, which takes the geometry and size of the by-pass opening into account. It is shown that the pressure loss models can capture the CFD results for each of the three pig geometries. The pressure loss models can be combined with pig/pipe-wall friction models to predict the velocity of a by-pass pig in a single phase pipeline, which is important for a safe and effective pigging operation. The applied building block approach may also be suitable to characterize pressure loss coefficients of complex geometries in general.

1. Introduction

In the oil and gas industry, pipeline networks are used to transport production fluids from wells to production plants. During normal operation, these pipelines need regular cleaning and inspection. Ideally, this pipeline maintenance should interrupt the production as little as possible. Typically, pipeline maintenance is done with a pig (Pipeline Inspection Gauge). This is a cylindrical or spherical device that is launched at the inlet of the pipe and subsequently travels through the pipeline while being propelled by the production of fluids. The pig is trapped in a receiver at the end of the pipeline. While a conventional pig completely seals the pipeline and travels with the same velocity as the production fluids, a by-pass pig has an opening hole which allows the production fluids to partially flow through the pig body. Fig. 1a shows an example of a by-pass pig. A by-pass pig will typically travel with a lower pig velocity compared to a conventional pig that completely seals the pipeline, as the velocity of the by-pass pig is not dictated by the velocity of the production fluids anymore, but depends on the overall force balance for the pig. In steady state this means that the driving pressure force F_p of the production fluids balances with the frictional force F_{fric} of the pig with the pipe wall, see Fig. 1b. The driving pressure force F_p depends on the pressure drop Δp over the pig and is expressed as $F_p = \Delta p A_{pig}$, where A_{pig} is the frontal area of the pig (which is equal to the cross sectional area of the pipe).

The reduction of the pig velocity has proven to be beneficial for both inspection and cleaning purposes (Wu and van Spronsen, 2005; Money et al., 2012). In addition, a lower pig velocity is necessary for safe operation, as a too high pig velocity may damage the insides of the pipe or the pig itself. As the travel velocity of the by-pass pig is important for the efficiency and safety of the pigging operation, detailed knowledge of the pressure drop Δp over the pig is needed in order to predict its velocity. This study focuses on quantifying the pressure drop Δp over various types of by-pass pigs which is characterized by a pressure loss coefficient K, defined as:

$$K = \frac{\Delta P}{\frac{1}{2}\rho U_{bp}^2}, \tag{1}$$

* Corresponding author.
E-mail address: m.h.w.hendrix@tudelft.nl (M.H.W. Hendrix).

http://dx.doi.org/10.1016/j.petrol.2016.11.009
Received 7 July 2016; Received in revised form 5 October 2016; Accepted 11 November 2016
Available online 16 November 2016
0920-4105/

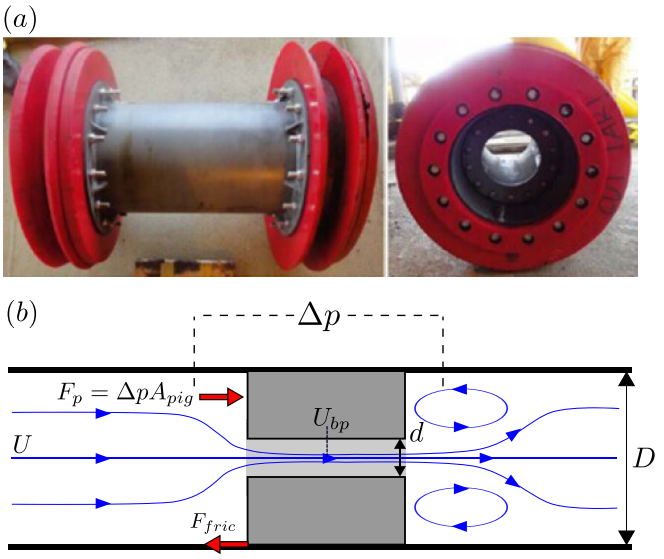

Fig. 1. (a) A bi-directional by-pass pig, taken from Lee et al. (2012). (b) A schematic of the forces on a by-pass pig in a horizontal pipeline. In steady state the driving force F_p due to the by-passing fluids is balanced by the frictional force F_{fric} of the pig with the pipe wall. In this schematic D indicates the pipe diameter, d the diameter of the by-pass hole, U the upstream bulk velocity, and U_{pig} the pig velocity.

where ρ is the density of the fluid and U_{bp} is the fluid velocity in the horizontal by-pass region relative to the pig motion, see Fig. 1. The pressure loss coefficient K depends on the size of the by-pass opening as well as on the design of the by-pass geometry, which may vary depending on the application of the pig. A good description of K is not only important for a steady state calculation of the pig velocity, but is also a relevant input parameter for 1D transient tools. Examples include 1D codes which are described in Nieckele et al. (2001), Tolmasquim and Nieckele (2008), Esmaeilzadeh et al. (2009), Jamshidi and Sarkari (2016) and commercial tools such as OLGA (Bendiksen et al., 1991) or LedaFlow (Goldszal et al., 2007), which are commonly used in the oil and gas industry. In these transient tools the trajectory of the pig through a pipeline can be monitored, and a relation for K needs to be known in advance. So far reliable correlations for K are missing, and the present study is aimed at providing one.

As the geometry of a pig varies depending on its application, a building block approach is used in order to provide a general framework for determining the corresponding pressure loss coefficient. The building block approach relies on a geometrical decomposition of the by-pass pig, and accounts for the contribution of the individual components of the by-pass pig geometry to the overall pressure loss. It is thus assumed that the flow patterns are uncorrelated between building blocks, i.e. the local flow pattern within a building block depends solely on geometrical characteristics of that building block. In order to validate the building block approach a CFD (Computational Fluid Dynamics) approach is applied to model fully turbulent single phase flow through various types of by-pass pigs. The bulk Reynolds number is fixed at $Re=UD/\nu = 10^7$, where ν is the kinematic viscosity of the fluid, U is the average velocity, and D is the pipe diameter. A similar Reynolds number has been used in a previous CFD study on by-pass pigs (Singh and Henkes, 2012), which allows for a direct comparison of the new results obtained in this work. From the CFD results the pressure loss coefficient K can be extracted.

The building block approach is tested on three different by-pass pig geometries encountered in the industry. First the relatively simple design of the bi-directional by-pass pig is revisited, which is shown in Fig. 1a. Furthermore, the by-pass pig shown in Fig. 2a is considered, which is referred to as the disk pig. This pig has a deflector plate, or disk, added at the exit of the by-pass pig. The deflector plate helps to get the pig into motion when the pressure drop over the pig is relatively

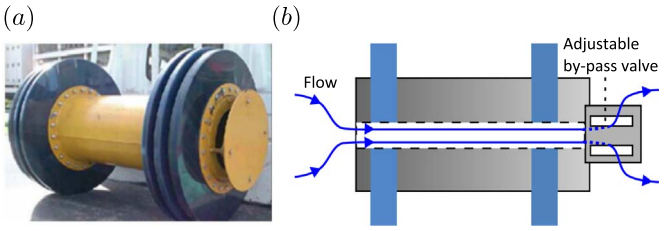

Fig. 2. (a) A by-pass pig with a deflector disk, taken from Wu and van Spronsen (2005). (b) Schematic of a by-pass pig with speed control. The by-pass valve can be adjusted to regulate the by-pass area.

small (Wu and van Spronsen, 2005). Finally, a by-pass pig design which is shown in Fig. 2b is considered. This by-pass pig has an adjustable by-pass area by making use of a rotatable valve. The angular position of the valve determines the opening of the by-pass holes. The adjustable by-pass enables control of the pressure drop over the pig and thus control of the speed of the pig. This by-pass pig is therefore referred to as the speed controlled pig. Examples of speed controlled pigs can be found in Thuenemann and Wegjan-Kuipers (2003) and Money et al. (2012).

The structure of the paper is as follows. In Section 2 a literature review is given on theory and correlations for by-pass pig geometries and the building block approach is explained. Section 3 describes the numerical setup which is used for the CFD calculations. Results obtained from the CFD simulations are discussed in Section 4. A summary of the results and possibilities for future research are given in Section 5.

2. Building block approach

In previous research the pressure loss coefficient of a bi-directional by-pass pig, K_{bidi}, was studied using CFD (Singh and Henkes, 2012). It was found that K_{bidi} can be successfully described by the Idelchik correlation for a thick orifice, as the bi-directional by-pass pig has a shape comparable with a thick orifice, see Fig. 1. For sufficiently thick orifices ($\frac{L_{pig}}{d} > 3$) the Idelchik correlation for a thick orifice reads (Idelchik, 1987):

$$K_{bidi} = 0.5\left(1 - \frac{A_0}{A_1}\right)^{0.75} + \frac{4fL_{pig}}{d} + \left(1 - \frac{A_0}{A_1}\right)^2, \tag{2}$$

where $A_0 = \frac{1}{4}\pi d^2$ is the cross-sectional area of the by-pass and $A_1 = \frac{1}{4}\pi D^2$ is the cross-sectional area of the pipe. The length of the pig is denoted by L_{pig} and f is the Fanning friction coefficient, which is determined by the Churchill relation (Churchill, 1977) using the Reynolds number defined in the horizontal by-pass area, that is $f = f(U_{bp}d/\nu)$. Here it is assumed that the walls of the by-pass area are hydrodynamically smooth, which implies that the friction factor is not a function of the wall roughness. This correlation for a thick orifice can be regarded as a linear combination of the loss associated with the inlet of the pig (contraction loss), the by-pass area of the pig (wall friction), and the outlet of the pig (expansion loss), see Fig. 3.

The use of this 'building block' approach to model the pressure loss coefficient of a by-pass pig has been suggested in previous work (Nguyen et al., 2001a, 2001b), and was validated recently with CFD for a bi-directional by-pass pig (Singh and Henkes, 2012; Azpiroz et al., 2015). In this paper it is attempted to use this building block approach for a more general class of by-pass pigs, namely the disk pig and the speed controlled pig, as depicted in Fig. 2. In order to model these more complex shaped pigs it is suggested to modify the last term of Eq. (4). This last term is associated with the pressure loss of a sudden expansion, which is also known as the Borda-Carnot equation. This equation holds very well for a fully turbulent flow (Teyssandier and Wilson, 1974; Massey, 2012). It is important to note that the Borda-Carnot equation, along with the other contributions in Eq. (2) are

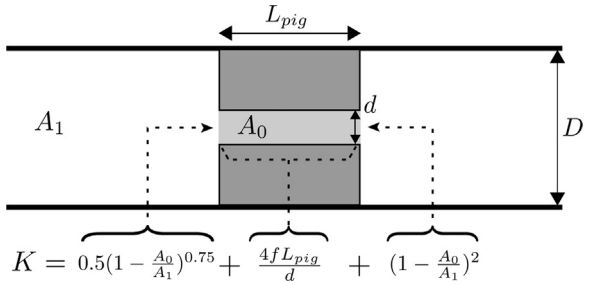

Fig. 3. Break down of the pressure loss coefficient of a bi-directional by-pass pig in a round pipe. Symbols are explained in the text.

associated with irreversible losses. It thus describes the change in total pressure P_t:

$$\Delta P_t = \frac{1}{2}\rho U_{bp}^2 K_{bidi} \tag{3}$$

As the pipe area is considered constant, the dynamic pressure upstream and downstream of the pig are equal. Therefore, the static pressure drop ΔP over the pig can be considered equal to the total pressure drop ΔP_t.

The fact that for both the disk pig and the speed controlled pig the exit of the pig can no longer be regarded as a sudden expansion emphasizes the need for a different correlation than Eq. (2). A new correlation for the disk pig and the speed controlled pig is now suggested.

2.1. Disk pig

In order to replace the last term in the original Idelchik correlation (2) the geometry of a disk valve depicted in Fig. 4a is considered first.

The geometry is taken from Idelchik (1987), in which the following correlation for the pressure loss coefficient of this geometry is proposed:

$$K_{dv} = \frac{2H}{d} + \frac{0.155d^2}{h^2} - 1.85. \tag{4}$$

This equation is reported to be valid within the range:

$$0.1 < \frac{h}{d} < 0.25, \tag{5}$$

and

$$1.2 < \frac{H}{d} < 1.5. \tag{6}$$

The validity of Eq. (4) outside this range has not been established. K_{dv} is associated with the velocity scale U_{bp}, see Fig. 4a. A schematic of the disk pig shown in Fig. 2a is depicted in Fig. 4b. The outlet of the disk pig can be represented by a disk valve as shown in Fig. 4a. The by-pass area of the disk pig A_{dv}, which is defined by the smallest by-pass area of the pig, is given by:

$$A_{dv} = \pi dh. \tag{7}$$

Replacing the last term of Eq. (2) with the loss coefficient of a disk

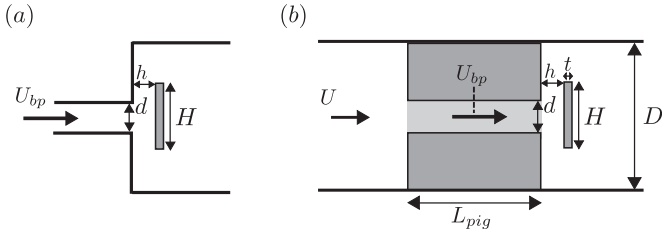

Fig. 4. (a) Disk valve geometry, adapted from Idelchik (1987) (b) Schematic of the disk pig.

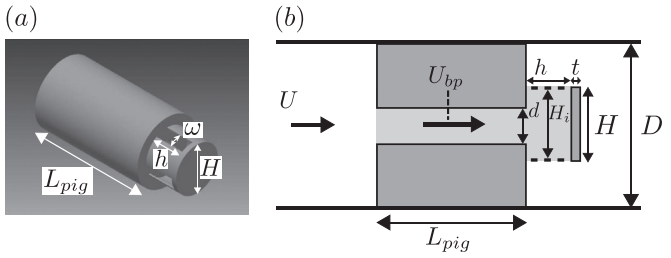

Fig. 5. (a) 3D schematic of the speed controlled pig. (b) Schematic of a cross-section of the speed controlled pig.

valve, Eq. (4), the following correlation for the pressure loss coefficient of a disk pig K_{dp} is proposed:

$$K_{dp} = 0.5\left(1 - \frac{A_0}{A_1}\right)^{0.75} + \frac{4fL_{pig}}{d} + \left(\frac{2H}{d} + \frac{0.155d^2}{h^2} - 1.85\right). \tag{8}$$

Note that the thickness of the disk t is not appearing in the proposed correlation. It is assumed that the flow is separating from the edge of the disk and will not reattach to the disk. This implies that the thickness is sufficiently small to neglect its influence on the flow.

2.2. Speed controlled pig

The speed controlled pig with a by-pass regulating valve as shown in Fig. 2b is modelled as a valve consisting of a disk with four adjustable opening slots, see Fig. 5a. The angle ω defines the opening angle of the slots in degrees. In Fig. 5b a cross-section of the speed controlled pig is shown.

The smallest by-pass area of the speed controlled pig A_{sp} is defined as:

$$A_{sp} = \pi H_i h \frac{n\omega}{360}, \tag{9}$$

where n=4 is the number of slots. No explicit relation for the pressure drop of such a geometry was found in the literature. As the speed controlled by-pass pig still resembles features of the geometry of the disk pig, the following correlation for the speed controlled pig is proposed:

$$K_{sp} = 0.5\left(1 - \frac{A_0}{A_1}\right)^{0.75} + \frac{4fL_{pig}}{d} + \left(\frac{2H}{d} + \frac{0.155d^2}{h_{eqv}^2} - 1.85\right). \tag{10}$$

Here h_{eqv} is the equivalent disk-to-pig distance such that the by-pass area of the speed controlled pig equals the by-pass area of a disk pig given by Eq. (7):

$$h_{eqv} = H^* \frac{h}{d} \frac{n\omega}{360}, \tag{11}$$

where H^* is the diameter of the slots, which can be taken as the inner diameter, $H^* = H_i$, or as the outer diameter $H^* = H$, see Fig. 5. Although this difference may be small in practice, these two approaches will both be treated and the result will be compared.

3. Numerical setup

This section deals with the numerical setup of the by-pass pig CFD model. In this research, all the CFD simulations are performed with ANSYS Fluent (version 14.5). The pig is modelled for operation at steady state with a constant pig velocity U_{pig}. To solve the flow around the pig the Reynolds-Averaged Navier-Stokes (RANS) equations are used. To close the RANS equations the realizable k-ϵ model is used. This turbulence model was tested in previous work and was found suitable to predict the re-attachment length of the flow in the wake of backward facing step (Singh and Henkes, 2012) as well as the pressure loss contribution of the different building blocks of the bi-directional

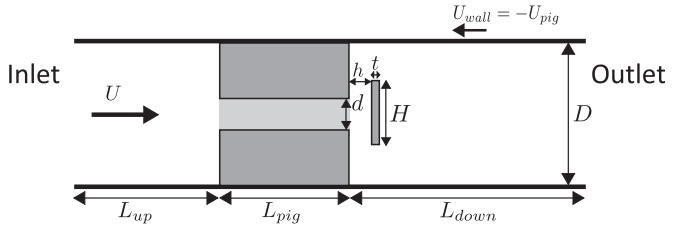

Fig. 6. Numerical setup. The inlet is located at the left. The equations are solved in a reference frame that moves with the pig. As a result, the pipe wall moves with a velocity $U_{wall} = -U_{pig}$.

pig (Azpiroz et al., 2015). Since the Reynolds number is high (Re=10^7) in the CFD calculations, standard wall functions are applied for the near wall region treatment. The effect of wall roughness is neglected. It is thus assumed that the walls are hydrodynamically smooth.

Fig. 6 shows a schematic of the numerical setup. The RANS equations are solved in a moving reference frame of the pig (Singh and Henkes, 2012; Azpiroz et al., 2015). This means that the walls have a nonzero velocity U_{wall} equal to $U_{wall} = -U_{pig}$. A User Defined Function (UDF) is applied at the inlet to prescribe a fully developed turbulent pipe flow profile. At the outlet a constant value for the static pressure is prescribed. In Fig. 7 the mesh that is used is shown. A structured mesh for all the simulations is employed which is constructed by dividing the domain in different sub-domains with a controlled number of nodes on each edge. This way the number and shape of the computational cells in each region can be controlled. Fig. 7b shows the mesh in the cross-sectional plane indicated by the dashed black line in Fig. 7a. An enlargement of the region within the white square in shown in Fig. 7c. The black arrow indicates a region of mesh refinement. The location of this mesh refinement corresponds to the radius of the horizontal by-pass area in order to refine the grid near the wall of the by-pass area. The same procedure is applied to the mesh at the inner pipe wall. The typical maximum value of y^+ in the simulation is around 4500, which is well within the range $30 < y^+ < 20000$ for which the flow is in the logarithmic layer, and standard wall function can be used to predict the velocity profile, see Fluent Theory Guide (2012) and Kundu et al. (2012).

4. Results

In this section the CFD results for the disk pig are discussed first. The obtained values for the pressure loss coefficient K are compared with the correlation suggested in Eq. (8). Next, the CFD results for the speed controlled pig are discussed. The obtained K values will be compared with Eq. (10). For the disk pig axi-symmetry is assumed and the CFD simulation is 2D, but for the speed controlled pig no axi-symmetry exists and the CFD simulation is 3D.

4.1. Disk pig

The flow around a disk pig has already been studied by Korban et al. (Azpiroz et al., 2015). In their study, the relation between the pressure loss coefficient K and the parameters which govern the disk pig model, was investigated. The K value of the disk pig was found to be around 2–3 times higher than the typical value that is found for a bi-directional pig (without disk). However, a general correlation to predict the pressure loss coefficient K for a disk pig was not given. Thus, in the present research, the flow around the disk pig is further investigated. Table 1 summarizes the key parameters which define a base case for the disk pig simulations. These parameters are based on a realistic scenario, which can be found in Wu and van Spronsen (2005). The parameters will be varied through using the following dimensionless numbers which define the disk pig geometry:

- Horizontal by-pass area fraction: $(\frac{d}{D})^2$
- Dimensionless disk height: $\frac{H}{D}$
- Disk by-pass area fraction: $\frac{4dh}{D^2}$

As discussed in Section 2, the effect of the dimensionless disk thickness t/D as well as the dimensionless pig length L_{pig}/D are not studied here.

First of all, the flow features of the disk pig are presented. Interestingly, two different types of flow behaviour around the disk pig have been observed in the simulation results. Secondly, various parameter studies are carried out, in order to study the relation between the pressure loss coefficient K and the governing parameters of the disk pig model.

4.1.1. Flow features of disk pig

Fig. 8 shows the streamlines that represent the mean flow around the disk pig. The fluid enters the pig through a sudden contraction. The flow behaviour in this region is similar to that of the conventional bi-directional pig (Azpiroz et al., 2015). After the horizontal by-pass region, the flow moves around the disk. In the disk by-pass region, the flow expands radially outward and has a jet-like structure. The flow subsequently detaches from the disk creating a recirculation zone downstream of the pig. To give insight in the pressure loss for the disk pig, the streamlines in Fig. 8 are colour coded with the local value of the total pressure coefficient C_{tp}. Here C_{tp} is defined as:

$$C_{tp} = \frac{P_t - P_{t_\infty}}{\frac{1}{2}\rho U_{bp}^2}, \tag{12}$$

where P_t is the local total pressure and P_{t_∞} is the total pressure downstream of the pig. As the total pressure is the sum of the static pressure and the dynamic pressure, C_{tp} can be associated with the irreversible losses in the system. As can be seen in Fig. 8, the recirculation zone is associated with dissipation in the flow, which is reflected in the low value of the total pressure coefficient C_{tp} after the flow has detached from the pig.

In general, two different types of flow behaviour are found. Fig. 8a shows the first flow behaviour. A jet is formed in the disk by-pass region. After the jet has moved away from the disk by-pass region, it first contacts the pig wall. Then, the jet moves along the pig wall towards the pipe wall. There is a small recirculation zone between the jet and the pig wall upstream of the disk. Another large recirculation zone is observed downstream of the disk. Fig. 8b shows the second flow behaviour around the disk pig. After the disk by-pass region, the jet does not first contact the pig wall, but it contacts the downstream pipe wall directly. Thus, the recirculation zone between the pig body and the jet is located in the corner of the pig wall and the downstream pipe wall. The main recirculation zone is still located downstream of the pig. In this research, the flow behaviours shown in Fig. 8a and b are referred to as “flow behaviour A” and “flow behaviour B”, respectively. Most importantly, the pressure drop across the disk pig is strongly dependent on the flow behaviour around it, which is reflected in the higher value of C_{tp} upstream of the pig for flow behaviour B compared to flow behaviour A.

Interestingly, the two flow solutions depicted in Fig. 8 are found for the same geometrical by-pass pig model subjected to the same boundary and inlet conditions. The equations thus allow for multiple steady state solutions. The applied parameters are as summarized in Table 1 but with a horizontal by-pass of 9% instead of 10%. The difference in steady state flow behaviour is caused, however, by a difference in initial condition. Flow behaviour A is part of the converged iterative solution of the steady state equations that are solved in Fluent using the default initialization scheme. Also another approach was taken in which the transient solver was used to reach steady state. In this case flow behaviour B was found. This solution was

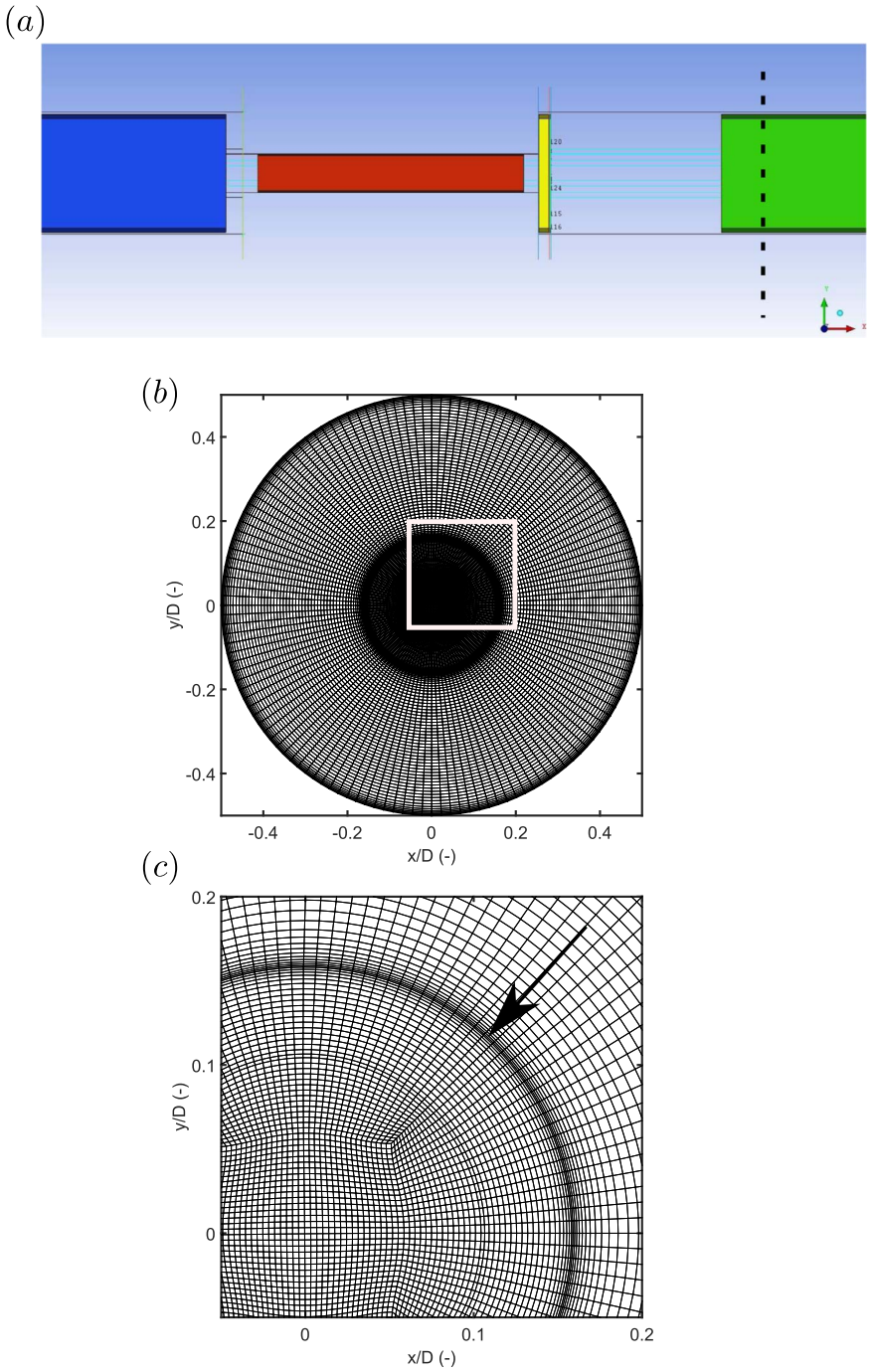

Fig. 7. (a) Blocks that represent different regions in streamwise direction. (b) Details of the mesh on the cross-sectional plane indicated by the dashed line in panel a. (c) Enlargement of the area indicated by the white square.

verified to indeed obey the steady state equations by initializing the steady state solver with flow behaviour B obtained from the transient simulation. Thus, for a disk pig model with certain governing parameters, two completely different numerical solutions can be achieved, and both solutions are in steady state. More details for the two solution region are provided in Appendix A. Multiple stable solutions for flow over a confined axisymmetric sudden expansion have been observed before, see for example Sheen et al. (1997). The direct attachment of the jet (behaviour A) can be induced by the Coanda effect and can cause hysteresis in the flow behaviour (Vanoverberghe et al., 2003; Tummers et al., 2009). According to the literature, it is also possible that an emerging jet in a confinement shows persistent oscillatory behaviour, instead of the two distinct steady states (Righolt et al., 2015). This oscillation, however, was not observed in the current study.

4.2. Parameter study

In this section the parameters which govern the disk pig model are varied to investigate the effect on the pressure loss coefficient K. Fig. 9a shows the value of C_{tp}, along the centreline of the disk pig shown in Fig. 8. The pressure loss coefficient K can now readily be determined:

$$K = C_{tp,up} - C_{tp,down}, \tag{13}$$

where $C_{tp,up}$ and $C_{tp,down}$ are the total pressure coefficients upstream and downstream of the pig, respectively. As was already shown in the previous section, flow behaviour B is associated with a higher loss

Table 1
Key parameters that govern the disk pig study.

Parameter	Value
Bulk velocity U	2.87 m/s
Horizontal by-pass area (%)	10%
Disk by-pass area (%)	8%
Pipe Diameter D	1.16 m
By-pass pig diameter d	0.3668 m
Upstream pipe length L_{up}	$5D$
Downstream pipe length L_{down}	$20D$
Pig length L_{pig}	2 m
Pig velocity	2 m/s
Distance between the pig body and the disk h	$0.06303D$
Disk diameter H	$0.396D$
Disk thickness t	$0.00862D$
Density ρ	68 kg/m^3
Viscosity μ	2.264 E-5 kg/ms
Reynolds number Re	1 E+7

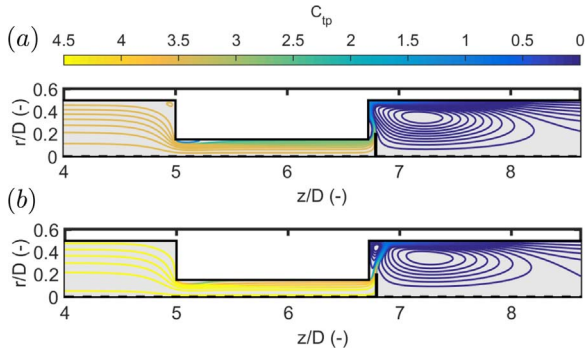

Fig. 8. (a) Flow behaviour A. (b) Flow behaviour B. The streamlines are colour coded by the value of the total pressure coefficient.

coefficient compared to flow behaviour A, which amounts to a difference of 30%. The effect of the dimensionless parameter $(d/D)^2$ on the two solutions and on K is also investigated by changing $(d/D)^2$ from 5% to 12.5%. This result is shown in Fig. 9b. The two solution region was found to be in the region:

$$7.8\% < \left(\frac{d}{D}\right)^2 < 11.3\%. \tag{14}$$

More details on the exploration of the two solution region can be found in Appendix A. Furthermore, the values of K obtained from the CFD simulations are compared with the correlation given by Eq. (8). Good agreement between the correlation for the disk pig and the CFD values was found, provided that the flow exhibits behaviour B.

Next, the effect of the disk diameter H is investigated through changing the dimensionless number H/D from 0.325 to 0.55, while keeping the other parameters fixed. Fig. 9c shows that when the disk has a relatively small disk height (when $H/D < 0.35$), the flow around the disk pig has behaviour B, while for $H/D > 0.375$, the flow around the disk pig has behaviour A.

The obtained CFD results are again compared with Eq. (8) (the latter is represented by the black solid line in Fig. 9c). Similar as was found for the parametric study of the horizontal by-pass area it can be concluded that Eq. (8) describes K_{dp} accurately if the flow around the disk pig has behaviour B. When H/D is larger than 0.375 and if the flow around the disk pig exhibits behaviour A, the pressure loss coefficient is found to have a constant value around $K_{dp} = 3.83$.

Finally, the parameter study of the disk by-pass area fraction $4dh/D^2$ is carried out. In this parameter study, the parameters are again kept fixed as shown in Table 1, and change the distance between the pig body and the disk h, in order to change the dimensionless parameter disk by-pass area $4dh/D^2$ from 6% to 20%. Fig. 9d shows the result of the obtained loss coefficient K_{dp} as a function of the disk pig by-pass area $4dh/D^2$. It is found that when the parameter h is relative small (when $4dh/D^2 < 8\%$), the flow around the disk pig has behaviour A, and when $4dh/D^2 > 10\%$, it changes to behaviour B. Eq. (8) is represented by the black solid line. Similar as found in the two previous parameter studies, Eq. (8) can predict K_{dp} accurately if the flow around the disk pig has behaviour B. Even though the points with flow behaviour B are partially out of the range for which Eq. (8) is reported to be valid, good agreement with the CFD results is found.

4.3. Speed controlled pig

This section is focused on the pressure drop coefficient of the speed controlled pig with the geometry depicted in Fig. 5. For the speed controlled pig four by-pass adjusting holes are generated to represent the by-pass adjusting device (which gives the dimensionless parameter n=4). The angle of the by-pass adjusting holes ω is changed to represent the speed control process. Through changing ω the dimensionless number $\frac{4hH_i(n\omega/360)}{D^2}$ is changed. This number represents the by-pass area fraction of the holes of the speed controlled pig. This dimensionless number is additional to the ones which already have been studied for the disk pig in the previous section. The effect of this dimensionless number on the pressure loss coefficient of the speed controlled pig is studied for two base geometries: one with a horizontal by-pass area of 10% and one with a horizontal by-pass area of 30%. The specific parameters of these two models are summarized in Table 2. The other parameters used in the simulation are unchanged with respect to the ones used in the previous section and can be found in Table 1. The maximum opening angle of the by-pass holes is 45 degrees. This means that the total opening with 4 holes is 180 degrees which is the maximum that can be achieved with a rotating valve. The distance of the disk to the pig body is matched in such a way that for an opening angle ω=45° the by-pass area of the holes is equal to the horizontal by-pass area. When the holes close, the by-pass area of the holes decrease, and will be smaller than the horizontal by-pass area. This ensures that the main pressure drop occurs through the holes, which enables control over the pressure loss as intended. As a consequence the maximum velocity in the system will always be located at the by-pass holes.

Fig. 10 shows a typical result obtained for the flow around the speed controlled pig. This model has a horizontal by-pass area of 30% and the opening angle of the holes ω is 45 degrees. As can be seen from Fig. 10a, the jets formed in the by-pass adjusting holes contact the pipe wall directly, and there is a recirculation zone both at the corner of the pig body and at the pipe wall. This is thus similar to flow behaviour B for the disk pig. This flow behaviour is observed for all the cases which were investigated for the speed controlled pig. This is mainly due to the location of the disk, which is typically placed at a larger distance from the pig body for the speed controlled pig compared to the disk pig. The main recirculation zone is in the downstream pipe and is much more complex than in the disk pig case. This is because there are four three-dimensional main jets formed in the four by-pass adjusting holes, and when the jets bend around the disk, the jet-like flow mixes again in the downstream pipe. A close up of the jets emerging from the by-pass holes is depicted in Fig. 10b. Similar to the disk pig, the main pressure drop occurs at the exit of the by-pass pig, which is shown by the streamlines which are colour coded with the value of the total pressure coefficient.

Next, a parameter variation of the two by-pass geometries listed in Table 2 is carried out. As the maximum velocity is always located in the holes it is intuitive to use this velocity to scale the pressure drop coefficient. Note that until now, the velocity in the horizontal by-pass area U_{bp} has been used to scale the pressure drop. Therefore, a modified pressure loss coefficient K' is defined which uses the velocity in the holes as a velocity scale. K' can thus be related to K as:

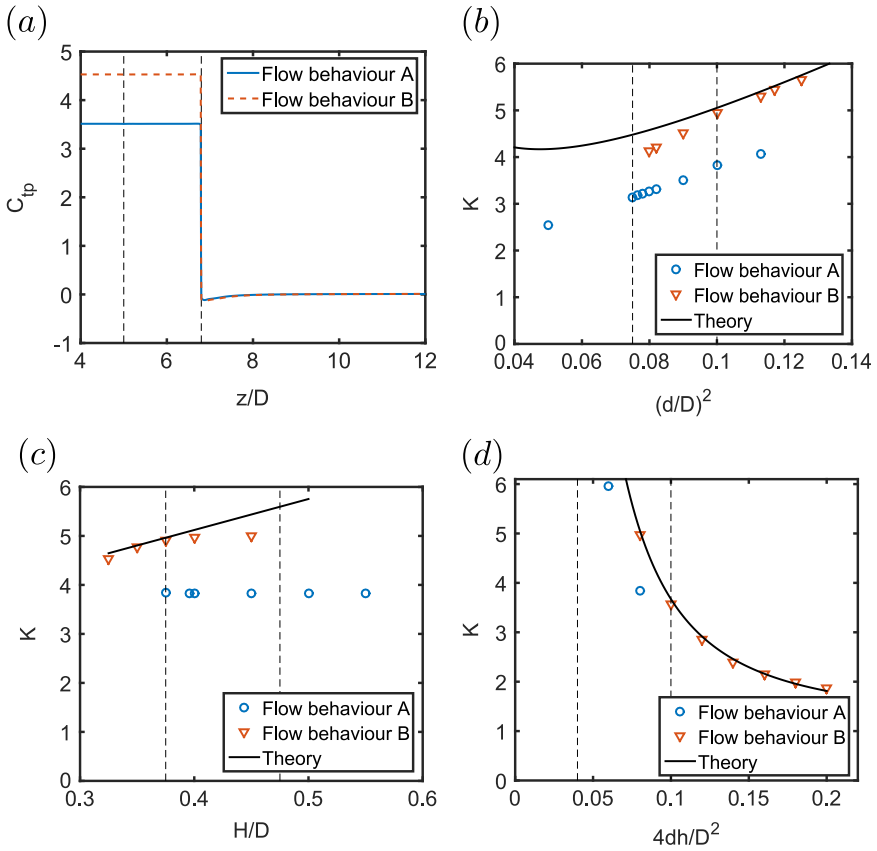

Fig. 9. (a) Total pressure coefficient along the centerline. (b) Pressure loss coefficient as function of the horizontal by-pass area $(d/D)^2$. (c) Pressure loss coefficient as function of H/D (d) Pressure loss coefficient as function of the disk by-pass area $4dh/D^2$. Values between the vertical dashed lines in b-d indicate the validity of Eq. (8).

Table 2
Key parameters that govern the speed controlled pig study.

Parameter	Geometry 1	Geometry 2
Horizontal by-pass area (%)	10%	30%
by-pass pig diameter d	0.3668 m	0.6354 m
Upstream pipe length L_{up}	$2D$	$2D$
Distance between the pig body and the disk h	$0.1118D$	$0.2236D$
Disk diameter H	$0.4835D$	$0.7071D$
Inner diameter holes H_i	$0.4472D$	$0.4472D$
Disk thickness t	$0.07071D$	$0.07071D$
Number of holes n	4	4

$$K' = \left[\frac{4hH_i(n\omega/360)}{d^2}\right]^2 K. \tag{15}$$

The parametric study is carried out by choosing the following values for ω: 11.25°, 22.5°, 37.75° and 45°. The results are depicted in Fig. 11.

It is noted that for ω=45° the by-pass area of the holes is equal to the horizontal by-pass area. In addition, the proposed correlation Eq. (10) is included. This correlation is based on treating the speed controlled pig as an effective disk pig, as explained in Section 2. The proposed correlation, despite the simplified approach, is able to predict the right trend that is given by the CFD results. However, especially for lower values of the by-pass area, the suggested correlation overpredicts the results. Nonetheless the correlation can help to give a first estimation of the pressure loss coefficient of a speed controlled pig with a geometry as approximated by the schematic as shown in Fig. 5.

5. Conclusions

In this paper a building block approach was applied to describe the pressure loss coefficient K of various by-pass pig geometries. First of all, K of the conventional bi-directional by-pass pig has been revisited. Subsequently, new correlations for more complex geometries have

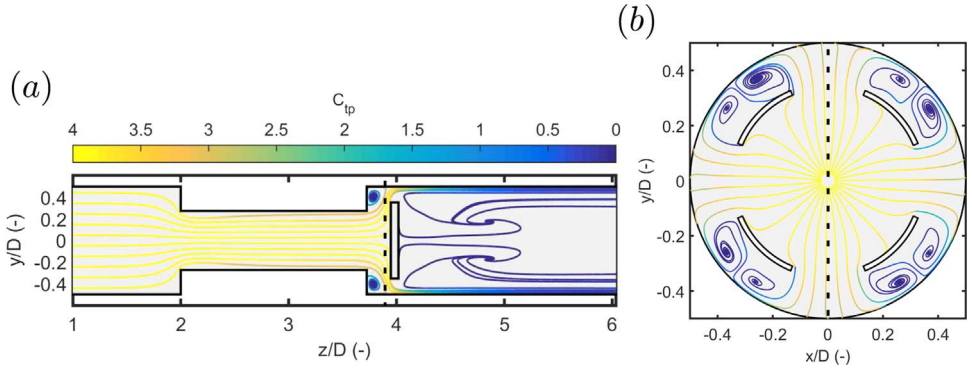

Fig. 10. (a) Streamlines around the speed controlled pig. (b) Streamlines in the region of the by-pass holes. The dashed black line indicates the same position in both panels.

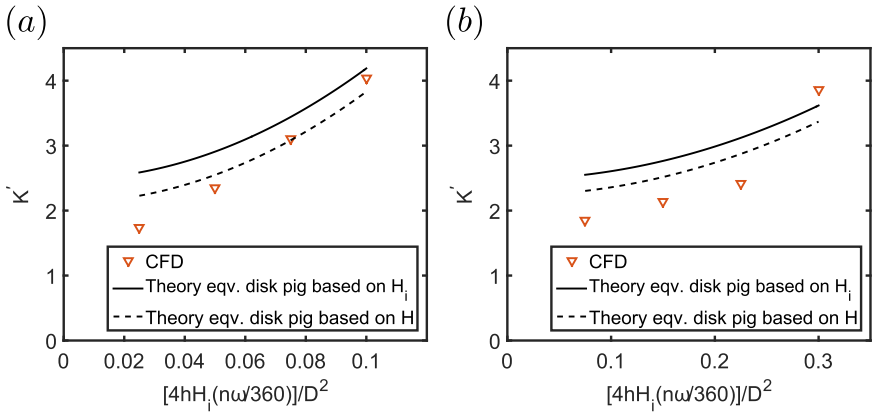

Fig. 11. (a) Pressure loss coefficient as function of the by-pass area fraction of the holes for a horizontal by-pass area fraction of 0.1. (b) Pressure loss coefficient as function of the by-pass area fraction of the holes for a horizontal by-pass area fraction of 0.3.

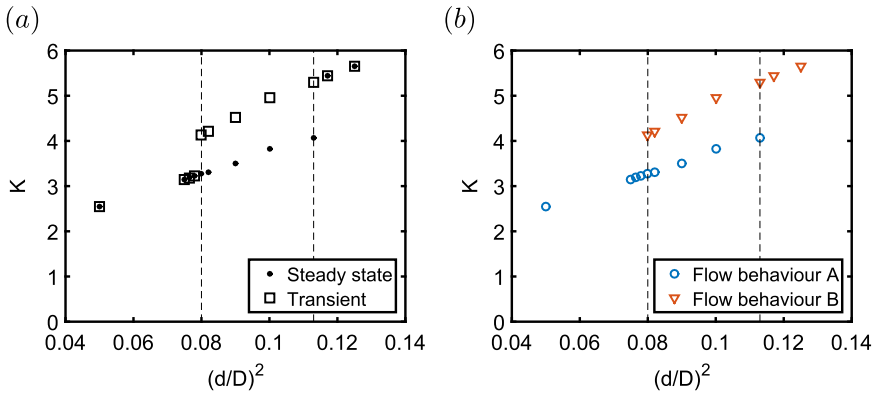

Fig. A1. Pressure loss coefficient. (a) Comparison between steady state and transient approach. (b) Comparison between flow behaviour A and B.

been proposed and compared with CFD simulations using the building block approach. This building block approach allowed to construct correlations and for the disk pig geometry and the speed controlled pig geometery. A two solution region was found for the disk pig geometry, which means that there are two stable flow behaviours (type A and type B) within the RANS framework of the current study. Good agreement was found between the proposed correlation for the disk pig and the CFD results, provided that the flow exhibits flow behaviour B. In addition, the pressure loss coefficient of the speed controlled pig was characterized. It was found that a correlation based on an equivalent disk pig gives qualitatively the right trend, but deviates quantitatively for small opening angles of the holes of the speed controlled pig. Further research is needed to predict K also for small opening angles of the holes. It is also of interest to further investigate the two solution region that was found for the disk pig. The boundary of the two solution region may be sensitive to the parameters of the RANS model, most notably the turbulence model. It would also be interesting to investigate the existence and stability of the two solution region experimentally in order to further verify the CFD modelling. The proposed building block approach has been successfully applied to describe the pressure loss coefficient of various by-pass pig geometries, and may also be applied to systematically model the pressure loss coefficient of complex flow geometries in general.

Acknowledgements

The work by the first author was funded by Shell Projects and Technology (PT35812), for which they are greatly acknowledged.

Appendix A. Two solution region

The two solution region in this work is explored by varying the initialization of the solver. Two different approaches are employed. In the first approach the steady state solver is initialized by the default initialization scheme in Fluent (Fluent Theory Guide, 2012). The second approach relies on running a transient simulation until steady state is reached. After the steady state is reached, this solution is used to initialize the transient simulation. In this way it can be verified that the steady state is stable. When these two approaches are applied within the two solution region, the first approach will trigger flow behaviour A, while the second approach will trigger flow behaviour B. This is shown in Fig. A1, in which the results from Fig. 9b are taken as an example. The two solution region is indicated by the dashed lines. Fig. A1a shows that outside the two solution region the steady state approach yields the same result as the transient approach.

References

Ansys Inc., Fluent Theory Guide, 14th Edition.
Azpiroz, J.E., Hendrix, M.H.W., Breugem, W.P., Henkes, R.A.W.M., 2015. CFD

modelling of bypass pigs with a deflector disk. In: Proceedings of the 17th International Conference on Multiphase Technology, pp. 141–155.
Bendiksen, K.H., Malnes, D., Moe, R., Nuland, S., 1991. Dynamic two-fluid model OLGA. Theory and application. SPE Prod. Eng. 6 (2), 171–180.
Churchill, S.W., 1977. Friction-factor equation spans all fluid-flow regimes. Chem. Eng. 84 (24), 91–92.
Esmaeilzadeh, F., Mowla, D., Asemani, M., 2009. Mathematical modeling and simulation of pigging operation in gas and liquid pipelines. J. Pet. Sci. Eng. 69 (1–2), 100–106.
Goldszal, A., Monsen, J.I., Danielson, T.J., Bansal, K.M., Yang, Z.L., Johansen, S.T., Depay, G., 2007. LedaFlow 1D: simulation results with multiphase gas/condensate and oil/gas field data. In: Proceedings of the 13th International Conference on Multiphase Production Technology, pp. 17–31.
Idelchik, I.E., 1987. Handbook of Hydraulic Resistance 2nd edition. Hemisphere Publishing Corporation.
Jamshidi, B., Sarkari, M., 2016. Simulation of pigging dynamics in gas-liquid two-phase flow pipelines. J. Nat. Gas Sci. Eng. 32, 407–414.
Kundu, P.K., Cohen, L.M., Dowling, D.R., 2012. Fluid Mechanics 5th edition. Academic Press.
Lee, H.S., Agustiawan, D., Jati, K., Aulia, M.A.H., Thomas, S.A., Appleyard, S.P., 2012. By-pass pigging operation experience and flow assurance study. In: Offshore Technology Conference, pp. 1–10.
Massey, B.S., 2012. Mechanics of Fluids 9th edition. Spon Press.
Money, N., Cockfield, D., Mayo, S., Smith, G., 2012. Dynamic speed control in high velocity pipelines. Pipeline Gas J. 239 (8), 30–38.
Nguyen, T.T., Yoo, H.R., Rho, Y.W., Kim, S.B., 2001a. Speed control of pig using bypass flow in natural gas pipeline. IEEE Int. Symp. Ind. Electron. 2, 863–868.
Nguyen, T.T., Kim, S.B., Yoo, H.R., Rho, Y.W., 2001b. Modeling and simulation for pig with bypass flow control in natural gas pipeline. KSME Int. J. 15 (9), 1302–1310.
Nieckele, A.O., Braga, A.M.B., Azevedo, L.F.A., 2001. Transient pig motion through gas and liquid pipelines. J. Energy Resour. Technol. Trans. ASME 123 (2–4), 260–268.
Righolt, B.W., Kenjereš, S., Kalter, R., Tummers, M.J., Kleijn, C.R., 2015. Dynamics of an oscillating turbulent jet in a confined cavity. Phys. Fluids 27.
Sheen, H.J., Chen, W.J., Wu, J.S., 1997. Flow patterns for an annular flow over an axisymmetric sudden expansion. J. Fluid Mech. 350, 177–188.
Singh, A., Henkes, R.A.W.M., 2012. CFD modelling of the flow around a by-pass pig. In: Proceedings of the 8th North American Conference on Multiphase Technology, pp. 229–243.
Teyssandier, R.G., Wilson, M.P., 1974. An analysis of flow through sudden enlargements in pipes. J. Fluid Mech. 64 (1), 85–95.
Thuenemann, U., Wegjan-Kuipers, J., 2003. Control your speed. World Pipelines 3 (3), 31–32.
Tolmasquim, S.T., Nieckele, A.O., 2008. Design and control of pig operations through pipelines. J. Pet. Sci. Eng. 62 (3–4), 102–110.
Tummers, M.J., Hübner, A.W., van Veen, E.H., Hanjalić, K., van der Meer, T.H., 2009. Hysteresis and transition in swirling nonpremixed flames. Combust. Flame 156 (2), 447–459.
Vanoverberghe, K.P., Van Den Bulck, E.V., Tummers, M.J., 2003. Confined annular swirling jet combustion. Combust. Sci. Technol. 175 (3), 545–578.
Wu, H.L., van Spronsen, G., 2005. Slug reduction with high by-pass pigs – a mature technology. In: Proceedings of the 12th International Conference on Multiphase Production Technology, Barcelona, pp. 313–325.